Hydrodynamic influence on the aggregation of colloids with short-range depletion potential in dilute suspensions

Adolfo Vázquez-Quesada* and Rafael Delgado-Buscalioni†
Department of Theoretical Condensed Matter Physics, Universidad Autónoma de Madrid, 28049 Madrid, Spain

(Received 23 April 2019; accepted 4 March 2020; published 21 May 2020)

This work studies the aggregation of colloids under depletion attraction focusing on the effect of hydrodynamic interactions on cluster kinetics and average structures. Our numerical study is based on a variant of the immersed boundary method (inertial coupling method) which solves the solvent fluctuating hydrodynamics and instantaneously couples the particle and the fluid momentum transfer. Comparison is made with Langevin dynamics and Monte Carlo methods, which do not include hydrodynamics. We consider a small system (20 and 40 particles) which reproduces the system considered by Whitmer and Luijten [J. Phys. Chem. B **115**, 7294 (2011)] (analyzed by multiparticle rotation dynamics). In that work, the authors report substantial hydrodynamic effects altering the cluster sizes and shapes. By contrast, within statistical error, we have not found any hydrodynamic effect on the average clusters structure. We also analyze the time-evolution of the aggregation kinetics, revealing a slowing down of the process due to the reduction of the mobility close to the clusters. The time correlation of the cluster number, shape, and size reveals two characteristic times: a decay at short times faster than the single-particle diffusion time t_D, followed by a slower exponential decay at long times with a typical time of several t_D.

DOI: 10.1103/PhysRevFluids.5.053301

I. INTRODUCTION

Understanding of aggregation of colloidal particles is of great interest in industrial applications and biological systems. Such a process can be controlled through changes in the effective interparticle potential. Given that the resulting structures are diffusing in a fluid, the influence of the hydrodynamic interactions look like a natural and relevant matter to figure out how the aggregation, percolation, and gel formation processes are affected by them. Because of the complexity of such systems, simulations show up as a relevant tool to approach the problem.

The first simulations on colloid aggregation modeled the colloid dynamics as a collection of independent Brownian walkers [1–5]. We will use "Brownian dynamics" (BD) to distinguish this approach from other methods including hydrodynamics. It is certainly computationally expensive to solve or model the correlations induced by hydrodynamic interactions. Probably for this reason, hydrodynamics has been neglected in the vast majority of computational studies. It was argued that the sole effect of hydrodynamics is to slow down the aggregation process, but *not* the topology of the aggregated structures at *long times*. Hydrodynamic interactions certainly alter the aggregation kinetics because they directly modify the colloidal mobility (which becomes a nonlocal collective property). However, in the case of reversible aggregation (moderate attractive energies $U < 5k_BT$) one expects the cluster statistics to be controlled by the free energy of the colloid phase (which

*adolfo.vazquez@uam.es
†rafael.delgado@uam.es

does not depend on hydrodynamics, as the Einstein relation proves). Following this argument, BD should be enough to capture the average cluster shape found in reversible aggregation. Aggregation, however, takes place in the unstable portion of the phase diagram (interaction energy versus colloidal volume fraction ϕ) and in some cases, like in a deep quench, the attraction energy is large ($U > 5k_BT$) and aggregation becomes irreversible. The role of hydrodynamics, both in reversible and irreversible aggregation is, however, still under debate. Partly because "irreversibility" is just an ideal, which in practice can only be defined in terms of some (long) observation time. As stated, hydrodynamic simulations are expensive and this fact shortens up the observation time, which is a source of misleading conclusions. Novel computational schemes and faster computer technologies will allow us to unfold the role of hydrodynamics on the evolution of colloidal aggregation.

In one of the earliest studies comparing 3D aggregation using BD and a hydrodynamic solver [6], particles were modeled using a smooth-profile representing the interface between particles and fluid phase [7]. Using short-ranged potentials and more than 2000 particles, these authors did not observed relevant differences between both methods, up to a volume fraction of $\phi \sim 0.3$. A subsequent work by Furukawa *et al.* [8] disagree with these findings: the fluid particle dynamics method (FPD) revealed different cluster statistics when compared with BD. Using a similar number of particles, volume fraction, and potential interaction they found that gelation (colloid network-forming) is favored if the hydrodynamic interactions are considered. They explain such a difference as an effect of the incompressible nature of the solvent, which generates a transversal flow when two colloids are approaching, even changing the dynamics of small clusters located initially in an icosahedron, $N = 13$, where N is the number of particles of such an aggregate. Another work by Whitmer and Luijten [9] confirmed such appealing conclusion, by comparing multiparticle collision dynamics (MPC) with Langevin Dynamics (LD) in small systems with a *total* number of particles $N_T = 20$, with depletion (short-ranged) potentials. Surprisingly, even at low volume fractions ($\phi \sim 0.025$), the hydrodynamic interactions introduced by MPC lead to different cluster shapes and size distribution, compared with those with LD (no hydrodynamics). However, the study on the influence of hydrodynamics on the clusters average asphericity in Ref. [9] were somewhat contradictory: Hydrodynamics tend to form more spherical clusters for $U \sim 3k_BT$, while more elongated structures for $U \sim 4.7k_BT$ and it was found to have little effect for $U \sim 6k_BT$. The second virial coefficient was introduced as a key factor determining the type of aggregation of colloids, in agreement with other works [10].

The influence of hydrodynamics in the kinetics of the gelation process was studied in detail in Ref. [11]. As the aggregation process advances in time, two different regimes were distinguished. In the initial regime, when the particles were aggregating in small clusters, hydrodynamics slows down the generation of such structures, while in the second regime where clusters are merging, hydrodynamics accelerates the process. This is due to the artificial slowing down of the diffusion coefficient $D_N \sim 1/N$ of a cluster of size N formed by independent Brownian walkers. In reality, the hydrodynamic drag on a cluster of radius $R(N)$ leads to $D_N \sim 1/R(N) \sim N^{-\nu}$, where ν is the fractal dimension of the cluster ($\nu \sim 0.35$ for globularlike clusters). This effect was observed to increase with the volume fraction. In Ref. [12] BD is compared with stochastic rotation dynamics (SRD is similar to MPC) coupled to molecular dynamics (SRD-MD) to find that the gelation (cluster percolation) threshold decreases when hydrodynamics is considered. It was also found that hydrodynamic effects diminish when the attractive potential is made stronger, but it creates more elongated clustering structures. Similar conclusions have been observed when comparing FPD and BD [13]. The effect of long-range potentials with repulsive barrier has been also studied [14–16], and similar observations about differences in the percolation threshold have been claimed.

In view of such disparity of conclusions and simulation methodologies, in this work we start a first step toward a revision of the subject. To that end, we deploy the inertial coupling method (ICM) [17], which consists on a version of the immersed boundary method where the fluctuating hydrodynamics of the solvent are explicitly solved using a finite-volume scheme, while particles and fluid are instantaneously coupled via conservation of momentum. In a thermal environment, such coupling guarantees that fluctuation-dissipation balance is respected without the need of an extra

dissipative channel for the particle (the noise acts on the fluid phase as a random stress). Particle fluctuations in velocity and position follow the Gibbs-Boltzmann statistics, as they should [17]. We compare ICM with Langevin (LD) and Monte Carlo (MC) simulations, where hydrodynamic interactions are lacking. These two models (LD and MC) differ in their dynamics, in the sense that LD simulations can be mapped to a real "time," by assigning the (single-particle) LD friction coefficient ξ to the Stokes friction coefficient $6\pi\eta R$ (where R is the particle radius and η the fluid viscosity). We note that in the ICM method, the Stokes friction coefficient is not an input, but naturally arises from the dynamics (the input parameters in ICM being simply R and η).

In this work, we consider the same system used in Ref. [9], where a small number of particles interact with a short-range potential in a periodic box with a low volume fraction $\phi \sim 0.025$. Our results, are however quite different as we did not find any significant change in the cluster average structures owing to the presence of hydrodynamics. We also considered the temporal evolution of the aggregates only to confirm the slowing down caused by the hydrodynamic interactions. We also detect two different time scales in the time correlation of the aggregate size and shape, characterizing short and long time processes. The paper is structured as follows: in Sec. II the system is described. In Sec. III the different methods of simulation which have been used are explained. In Sec. IV the numerical results are presented: time-independent results in Sec. IV A and time-dependent results in Sec. IV B. Finally, the conclusions are exposed in Sec. V.

II. THE SYSTEM

Our system is a colloidal suspension of particles of radius R immersed in a solvent with depletants (usually globular polymers in experiments). We do not resolve the depletant dynamics and approximate the colloid free energy by a pair-wise interaction taken from the Asakura-Oosawa theory [18]. In particular, following Ref. [9], we use the Asakura-Oosawa-Vrij potential U_{AOV} combined with a (steric) repulsive $1/r^{36}$ potential U_{ss}, where r is the distance between particles,

$$U(r) = U_{\mathrm{ss}}(r) + U_{\mathrm{att}}(r), \tag{1}$$

being

$$U_{\mathrm{ss}}(r) = \frac{\alpha_1}{\beta}\left(\frac{1}{r^{36}} - \frac{2}{\alpha_2^{18} r^{18}} + \frac{1}{\alpha_2^{36}}\right) \tag{2}$$

and

$$U_{\mathrm{att}}(r) = \begin{cases} \frac{1}{\beta}[B(r-\sigma_{\mathrm{cc}})^2 + C], & \text{if } 0 < r < (1+\alpha_3\zeta)\sigma_{\mathrm{cc}}, \\ U_{\mathrm{AOV}}(r), & \text{if } (1+\alpha_3\zeta)\sigma_{\mathrm{cc}} \leqslant r < \alpha_2. \end{cases} \tag{3}$$

The range of attraction of the depletion potential is determined by the parameter $\zeta \equiv 2R_g/\sigma_{\mathrm{cc}}$, where R_g is the radius of gyration of the depletant, and σ_{cc} the colloidal diameter. The strength of the depletion is controlled by ζ and the polymer concentration ϕ_p. The cutoff radius of the depletion is given by $\alpha_2 = (1+\zeta)\sigma_{\mathrm{cc}}$. Temperature is introduced through the usual parameter $\beta = \frac{1}{k_B T}$, where k_B is the Boltzmann's constant and T the temperature. To ensure that the potential is smooth at its cutoff radius, the repulsive term has been supplemented by a $1/r^{18}$ term, and the amplitude α_1 of the repulsive force is considered equal to $\sigma_{\mathrm{cc}}^{36}$. The AOV depletion potential has been modified with a quadratic term to avoid singularities in the range of interaction. The crossover with the added term is determined by α_3. The constants B and C are calculated to get a continuous and differentiable potential

$$\begin{aligned} B &= \frac{1}{\beta}\frac{3\phi_p}{4\alpha_3\zeta^4\sigma_{\mathrm{cc}}^2}[(1+\zeta)^2 - (1+\alpha_3\zeta)^2], \\ C &= U_{\mathrm{AOV}}[r = \sigma_{\mathrm{cc}}(1+\alpha_3\zeta)] - B(\alpha_3\zeta\sigma_{\mathrm{cc}})^2. \end{aligned} \tag{4}$$

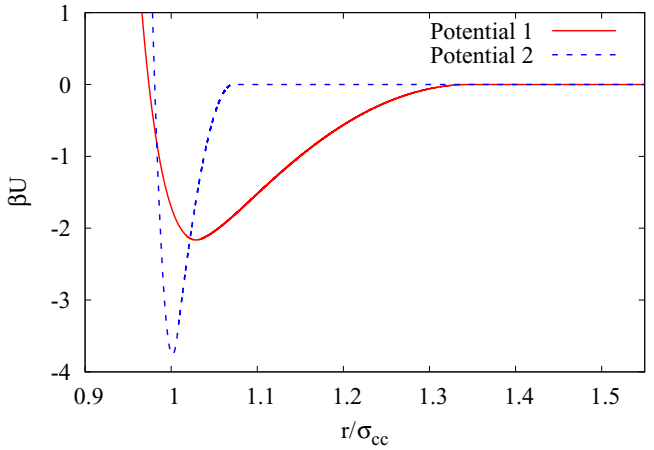

FIG. 1. Depletion potentials used in this work: see Table I for details.

The explicit expression of the AOV potential reads

$$U_{\mathrm{AOV}}(r) = \begin{cases} -\frac{1}{\beta}\phi_p\left(\frac{1+\zeta}{\zeta}\right)^3\left[1 - \frac{3r/\sigma_{\mathrm{cc}}}{2(1+\zeta)} + \frac{1}{2}\left(\frac{r/\sigma_{\mathrm{cc}}}{1+\zeta}\right)^3\right], & \text{if } 1 < r/\sigma_{\mathrm{cc}} < (1+\zeta), \\ 0, & \text{otherwise.} \end{cases} \tag{5}$$

The colloidal diameter of the potential is set to $\sigma_{\mathrm{cc}} = 4.3$, which is somewhat larger than the hydrodynamic diameter $2R = 3.64$. Two different potentials drawn in Fig. 1 have been considered, with the following parameters: $\zeta = 0.347$ and $\phi_p = 0.560$ (potential 1), and $\zeta = 0.072$ and $\phi_p = 0.216$ (potential 2). Both potentials have the same second virial coefficient. As done in Ref. [9], we will consider that the fluid density $\rho = 5$ is greater than the solid density $\rho_s = 3.0$. Temperature will be taken as $k_BT = 1$ and viscosity as $\eta = 2.49$ so the Schmidt number of one colloidal particle is given by $\mathrm{Sc} \approx 50$, which matches that of Ref. [9].

We consider the system in Ref. [9] which contains $N_T = 20$ particles (system 1) and yet another similar one with $N_T = 40$ (system 2) at the same volume fraction. The periodic cubic box used for system 1 has size $L = 32$ and $L = 40$ for system 2. We have performed $N_{\mathrm{sim}} = 9$ different simulations during a time $t \sim 1000\ t_D$, where t_D is the diffusion time of one single particle. The parameters of the system can be consulted in Table I.

III. METHODS OF SIMULATION

A simulation box of size L is considered, where N_T colloidal particles of radius R are diffusing in a solvent with density ρ and viscosity η. The particles are interacting through the depletion potential U_{att} described in Sec. II. Periodic boundary conditions are taken in each direction. The volume fraction of particles is calculated as $\phi = NV_{\mathrm{part}}/V_{\mathrm{total}}$, V_{part} being the volume of one single particle and $V_{\mathrm{total}} = L^3$ the total volume of the simulation box. As we have written before, three different models are considered to simulate the system: Langevin dynamics, Monte Carlo, and inertial coupling method.

A. Langevin dynamics

Langevin dynamics solves the dynamics of small particles in a solvent which creates a drag force to each particle and adds a random velocity leading to Brownian motion. The fluid drag is $-\xi\mathbf{v}_i$ so that particles do not interact hydrodynamically and mutual friction is neglected. The velocity relaxation rate $\gamma = \xi/m$ (where the particle mass is m) is directly related to the amplitude of the random force to ensure consistency with the equilibrium thermal average $\langle v_i^2\rangle = (3/2)k_BT/m$. This

TABLE I. Parameters of the model. The diffusion time $t_D = R^2/D$, where $D = k_BT/(6\pi\eta R)$ is the Stokes-Einstein diffusion coefficient and we work in $k_BT = 1$ units. Two different set of runs were performed using $N_{\rm sim} = 9$ long runs (over $1000\,t_D$) and another set with $N_{\rm sim} = 96$ shorter runs of $176\,t_D$.

R	1.82	
L	32 (system 1)	40 (system 2)
N_T	20 (system 1)	40 (system 2)
β	1	
η	2.49	
ρ	5	
ρ_s	3	
$t_{\rm sim}$	$\approx 1000\,t_D$ or $\approx 176\,t_D$	
$N_{\rm sim}$	9 or 96	
$\sigma_{\rm cc}$	4.3	
ϕ_p	0.560 (pot 1)	0.216 (pot 2)
ζ	0.347 (pot 1)	0.072 (pot 2)
α_3	0.1	
dt	0.01	
D	0.0117	

so-called fluctuation dissipation balance is ensured by adding time-uncorrelated Brownian jumps in velocity, $d\tilde{\boldsymbol{v}}_i(t) = \sqrt{2k_BT\gamma}\,d\boldsymbol{W}_i$, where $d\boldsymbol{W}_i(t)$ is a Wiener process (independent for each particle) whose variance is just the time step dt. Colloidal aggregation forces are represented by pair-wise attractive colloidal interactions $-\boldsymbol{\nabla}U_{\rm att}(|\boldsymbol{r}_j - \boldsymbol{r}_i|)$ where i and j indicate two whatever colloids,

$$m d\boldsymbol{v}_i = -\xi\,\boldsymbol{v}_i dt + m d\tilde{\boldsymbol{v}}_i(t) - \sum_{j\neq i} \boldsymbol{\nabla}U_{\rm att}(|\boldsymbol{r}_j - \boldsymbol{r}_i|)dt. \tag{6}$$

LD does not consider the solvent dynamics, which just appears in the friction coefficient ξ. To compare LD with ICM we use its Stokes form $\xi = 6\pi\eta R$.

B. Monte Carlo

Monte Carlo simulations are based on the Metropolis algorithm, which consists on a process which generates a sequence of states or system's configurations. In its steady state, this process samples the canonical Gibbs-Boltzmann distribution (proportional to $\exp[-\beta U^{(N)}(\{\mathbf{r}\})]$, where $U^{(N)}$ is the potential energy of the ensemble of N_T colloidal particles in a volume V at temperature T). Strictly speaking Monte Carlo simulations do not offer dynamic information, however, if the exploration of the phase space is carried out by simple translational random jumps of individual particles, MC becomes quite similar to a purely diffusive process of independent Brownian walkers. Here we use such procedure: Starting from a random configuration of particles, we move the system by changing randomly the position of one single particle at a time, as specified in Ref. [19].

C. ICM

ICM is a computational method to simulate suspensions with or without thermal fluctuations. In this method, the solvent dynamics is simulated by using a finite-volume method in a rectangular grid. Through a staggered scheme, the Navier-Stokes equations modeled by ICM read

$$\boldsymbol{\nabla}\cdot\boldsymbol{v} = 0, \tag{7}$$

$$\partial_t\boldsymbol{v} = -\boldsymbol{\nabla}\pi - \boldsymbol{\nabla}\cdot\boldsymbol{v}\boldsymbol{v} + \frac{\eta}{\rho}\nabla^2\boldsymbol{v} + \frac{1}{\rho}\boldsymbol{\nabla}\cdot(\sqrt{2\eta k_BT}\tilde{\boldsymbol{\mathcal{W}}}_{\boldsymbol{v}}), \tag{8}$$

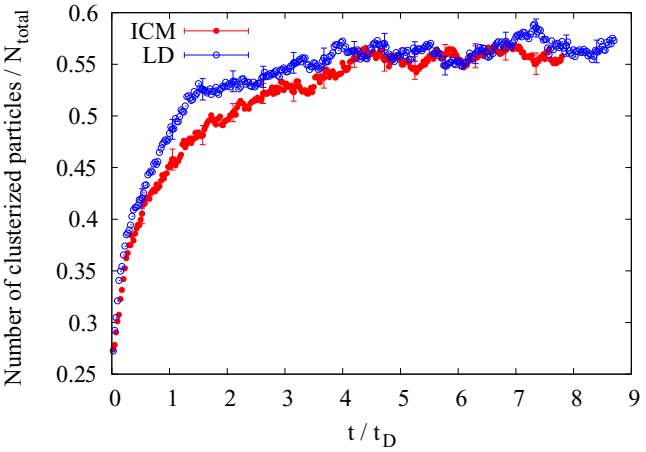

FIG. 2. Time evolution of the total clusterized mass (particles in clusters of size $N \geqslant 2$ in simulations with and without hydrodynamics (ICM and LD, respectively). Error bars represent the standard error.

where ρ and $\boldsymbol{v}$ are the density and velocity of the fluid and η its shear viscosity. π is the pressure, which is used as a Lagrange multiplier to ensure the free divergence condition Eq. (7). The noise term $\tilde{\boldsymbol{\mathcal{W}}}_{\boldsymbol{v}}$ is given by

$$\tilde{\boldsymbol{\mathcal{W}}}_{\boldsymbol{v}} = \frac{\boldsymbol{\mathcal{W}}_{\boldsymbol{v}} + \boldsymbol{\mathcal{W}}_{\boldsymbol{v}}^{T}}{\sqrt{2}}, \tag{9}$$

where $\boldsymbol{\mathcal{W}}_{\boldsymbol{v}}$ is an uncorrelated tensor of random Gaussian terms with the next covariance,

$$\left\langle \mathcal{W}_{v}^{ij}(\boldsymbol{r}, t)\mathcal{W}_{v}^{kl}(\boldsymbol{r}', t')\right\rangle = \delta_{ij}\delta_{kl}\delta(t - t')\delta(\boldsymbol{r} - \boldsymbol{r}'). \tag{10}$$

The particles are included through the immersed boundary method (IBM) [20] as Lagrangian points (blobs) that can freely move. The interaction between the Lagrangian particles and the Eulerian solvent is calculated via an interpolating kernel $\delta_a(\boldsymbol{r})$, which is bell-shaped and compact supported of size a [17]. Such a kernel is considered as a discrete approximation of the Dirac delta function. With this kernel we can perform two important operations to model a two-way coupling between the fluid and the blobs. On one hand, the local averaging linear operator $\boldsymbol{J}(\boldsymbol{q})$, $\boldsymbol{q}$ being the position of the blob, allows for the calculations of the local velocity $\boldsymbol{v}_q$ in the position of the blob,

$$\boldsymbol{v}_q(t) = \boldsymbol{J}\boldsymbol{v}(\boldsymbol{r}, t) = \int \delta_a(\boldsymbol{q} - \boldsymbol{r})\boldsymbol{v}(\boldsymbol{r}, t)d\boldsymbol{r}. \tag{11}$$

However, the local spreading linear operator $\boldsymbol{S}(\boldsymbol{q})$ transfers the force $\boldsymbol{F}(t)$ applied on the blob to the fluid as a smooth force density field $\boldsymbol{f}(\boldsymbol{r}, t)$,

$$\boldsymbol{f}(\boldsymbol{r}, t) = \boldsymbol{S}\boldsymbol{F}(t) = \boldsymbol{F}(t)\delta_a(\boldsymbol{q} - \boldsymbol{r}). \tag{12}$$

A no-slip constraint on the blob is imposed through an instantaneous coupling between the velocity of the fluid $\boldsymbol{v}$ and the velocity of the particle $\boldsymbol{u}$,

$$\boldsymbol{u} = \boldsymbol{J}\boldsymbol{v}(\boldsymbol{r}, t). \tag{13}$$

For further details about the incompressible ICM model, the reader is referred to Ref. [17].

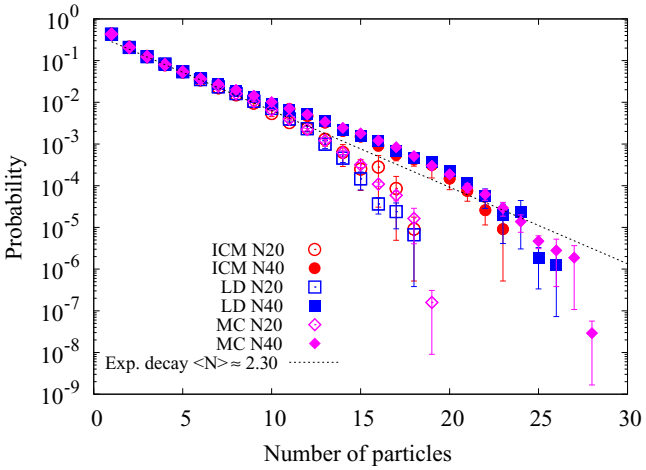

FIG. 3. Probability $P(N)$ defined by Eq. (14). Results for systems with 20 (open symbols) and 40 particles (closed symbols) are presented for ICM (red), Langevin dynamics (blue), and Monte Carlo (pink) simulations. Dashed line corresponds to $P(N) \approx \frac{1}{\langle N \rangle} \exp\left(-\frac{N}{\langle N \rangle}\right)$. The error bars represent the standard error.

IV. NUMERICAL RESULTS

A. Long time averages

This section focuses on statistical averages performed at long times, once the (reversible) aggregation process is settled to a stationary state. As shown in Fig. 2, a steady state is reached typically after a transient of about 10 t_D, once the average fraction of particles linked in some cluster reaches about half the total number of particles. To properly sample the steady state, we have performed $N_{\text{sim}} = 9$ simulations during a total simulation time of $\sim 1000 t_D$, where $t_D = R^2/D$

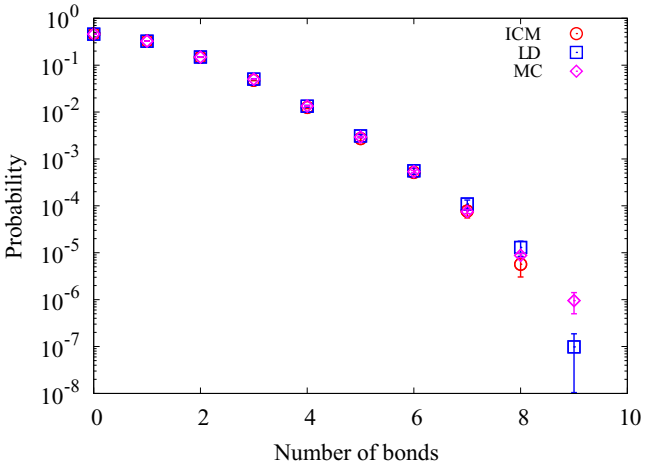

FIG. 4. Probability of the number of bonds per particle for a system with 20 particles interacting with the potential 1. Results are presented for ICM (red), Langevin dynamics (blue), and Monte Carlo (pink) simulations. The error bars represent the standard error. The average number of bonds in a cluster of size $N \geqslant 2$ is 1.55.

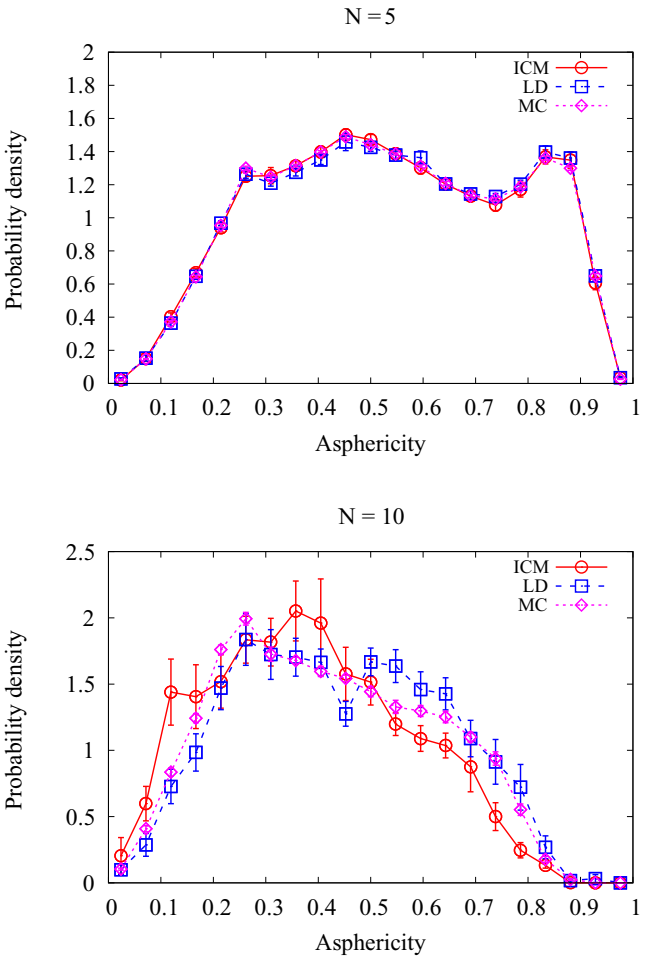

FIG. 5. Probability density of the asphericity for clusters of size $N = 5, 10$. Results are presented for ICM (red), Langevin dynamics (blue), and Monte Carlo (pink) simulations. The error bars represent the standard error. Results correspond to potential 1 in Fig. 1.

[with $D = k_B T/(6\pi\eta R)$] is the diffusion time of one particle. The total sampling time is similar to that used in Ref. [9] (96 simulations during $88t_D$).

We now consider the average distribution of cluster sizes in the stationary regime. A particle belongs to a cluster if it is located at a distance less than α_2 (potential range) of some other particle of the cluster. The probability of encountering a particle in a cluster of size N is given by

$$P(N) = \frac{n_N N}{\sum_{i=1}^{N_{\max}} i\, n_i}, \tag{14}$$

where n_i is the total number of clusters of size i, and $N_{\max} = N_T$ is the maximum possible size of a cluster.

In Fig. 3 the probability $P(N)$ is shown for the potential 1 (see Fig. 1) and two cases with 20 and 40 particles. Within statistical error, the results with and without hydrodynamics are similar. Note that the $P(N)$ obtained for increasing total number of particles (20 and 40) results to be similar for clusters of size $N < 10$ and reveals an exponential decay characteristic of a Poissonian process (reversible aggregation) $P(N) \approx 1/\langle N\rangle \exp[-N/\langle N\rangle]$ with an average cluster size of $\langle N\rangle = 2.30$

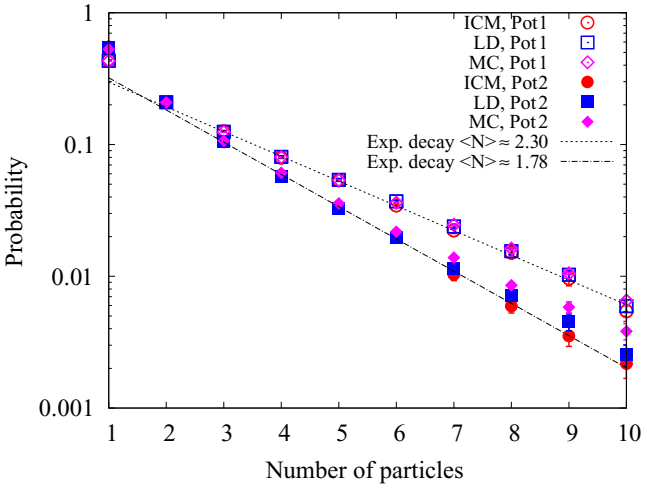

FIG. 6. Probability of cluster sizes with two different potentials (potential 1, open symbols, and potential 2, closed symbols) with the same second virial. Results are presented for ICM (red), Langevin dynamics (blue), and Monte Carlo (pink) simulations. The error bars represent the standard error.

(for potential 1). By contrast, the results presented in Ref. [9] indicate a significant larger probability of formation of large clusters when hydrodynamics is included.

We have not found either any relevant difference in the probability of the number of bonds per particle with and without hydrodynamics (Fig. 4). In contrast, in Ref. [9] the probability of having a large number of bonds is higher with hydrodynamics than without it.

The average shape of the clusters has also been studied by considering their asphericity A, calculated from their gyration tensor $\boldsymbol{T} = \sum_i \boldsymbol{r}_i \boldsymbol{r}_i$, where the index i goes over the particles belonging to the cluster, as [9]

$$\begin{aligned} R_g &= \sqrt{\mathrm{Tr}(\boldsymbol{T})}, \\ A &= \frac{1}{2}\frac{(\lambda_1-\lambda_2)^2+(\lambda_2-\lambda_3)^2+(\lambda_3-\lambda_1)^2}{R_g^4}, \end{aligned} \tag{15}$$

where R_g is the gyration radius, and λ_1, λ_2, and λ_3 the eigenvalues of the gyration tensor. In Fig. 5 the asphericity distributions for clusters of size 5 and 10 simulated with the three methods in the case of potential 1 have been drawn for the simulations with $N_T = 20$. Within the error of the values we do not find either a significant difference. By contrast, Ref. [9] reports contradictory results in this respect: Hydrodynamics would alter the average asphericity tending to form more spherical clusters for $U \sim 2k_BT$ (potential 1) while elongated structures for $U \sim 4.7k_BT$ (potential 2) (and little effect in the case of $U \sim 6k_BT$).

We note that potential 2 (see Table I) has the same value of the second virial coefficient as potential 1. Simulations with the potential 2 allow us to check to what extent the second virial is the leading parameter characterizing clustering [10]. As in Ref. [9] we find that the cluster probability of both potentials is not exactly the same (see Fig. 6). Small, but significant differences can be also observed in the profiles of asphericity versus the cluster size (Fig. 7, top). Such differences might result from the the fact that the interaction range of the potentials is not small enough for such statement to be valid. In any case, in contrast with Ref. [9], our simulations with and without hydrodynamics using the potential 2 yield similar results within statistical uncertainties [Figs. 5 (top) and 7 (bottom)].

To test the source of differences between our study and that in Ref. [9] we considered possible effects from finite sampling times. In Ref. [9] the sampling window (single-run time) was $88t_D$ while

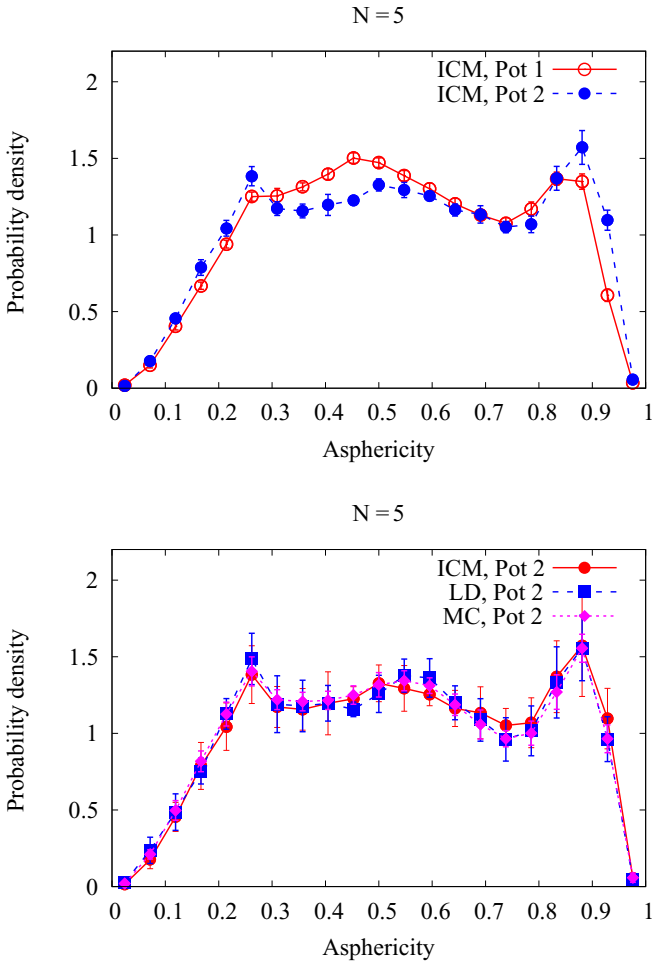

FIG. 7. Top: Probability density of the asphericity, obtained from ICM simulations, for clusters of size $N = 5$ with two different potentials with the same second virial: potential 1 (red) and potential 2 (blue). Bottom: The same quantity for the potential 2 from ICM (red), LD (blue), and MC (pink). The error bars represent the standard error.

we used $1000t_D$. While the *total* sampling time is similar in both studies (they used 96 simulations while we used 9), potential *transient* effects could affect results obtained with the smaller sampling window. To test this hypothesis, we have reproduced the same set of simulations performed using smaller windows of $176t_D$ (and 96 runs) and analyzed last $88t_D$ portion of each run (as in Ref. [9]). The resulting cluster probability $P(N)$, drawn in Fig. 8, do not show any significant difference with respect to the long-run case, neither using $N_T = 20$ or 40 particles.

B. Time correlations

This section studies the time correlation of several quantities in the stationary regime. We consider $N_T = 20$ particles and the potential 1.

The survival time of clusters of size N is an indicator of the dynamics of reversible aggregation. It is defined as the time lapse from the formation of the cluster until its disappearance, either because it has lost particles or, because it has grown. Given that we can not map the entire space

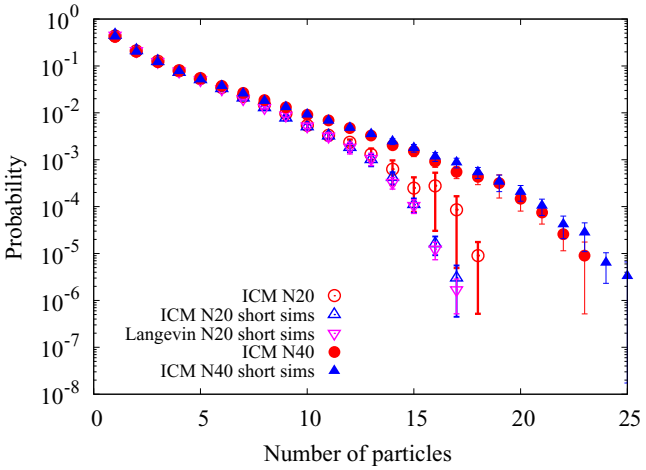

FIG. 8. Comparison between 9 long ($\approx 1000 t_D$) and 96 short simulations ($\approx 88 t_D$) (like Ref. [9]) for $N_T = 20$ and $N_T = 40$ simulations. The error bars represent the standard error.

of probabilities, we will define the probability density of survival time of clusters only until some cutoff time t_{cut}, which we consider to be large enough. In our case, $t_{\text{cut}} \approx 2.6 t_D$, t_D being the diffusion time of a single particle. In Fig. 9 we have drawn this quantity for clusters of size $N = 3,\ 5$, and 7 in ICM and LD simulations. We can see that the choice of t_{cut} is appropriate, given that the probability of a cluster to survive above $t = 0.1 t_D$ is extremely small (<0.02). The extremely fast decay in survival times at short time is due to Brownian fluctuations of satellite particles around clusters, leading to fast entry/departure events in and out the potential cut-off range. At somewhat longer times ($t > 0.2 t_D$) we detect a slower decay rate, which reveals that hydrodynamics slows down the aggregation dynamics (see Fig. 9), making the cluster survive for longer times.

Due to its sensitivity to fast entry/departure fluctuations, the survival time of a cluster is not the best way to investigate the aggregation dynamics at long times. A more informative quantity in this respect is the time-correlation of the number of clusters of size N:

$$c_N(t) = \langle (n_N(t + t_0) - \langle n_N \rangle)\,(n_N(t_0) - \langle n_N \rangle) \rangle. \tag{16}$$

Note that $c_N(t)$ is sampling a collective dynamics which does not distinguish between individual cluster survivals. $c_N(t)$ is not sensible to fast entry/departure fluctuations, which are simply averaged in large lag-times t. Figure 10 draws $c_N(t)/c_N(0)$ obtained from ICM simulations. It gives us an idea on the rate at which the system *updates* the number of clusters of size N. From Fig. 10 one infers two different regimes. At short times (in fractions of t_D) the size of the clusters rapidly reorganizes at a rate which increases with the cluster size. This regime reflects escape and re-entry events of satellite particles at the surface of the clusters, connected to the cluster by a single bond. We note that the Kramer escape time [21][1] for a colloid connected with a single bond with the potential 1 is $\tau_E \approx 0.98\, t_D$ and, obviously, the number of escape events (so thus the net escape rate) increases with the number of particles in the cluster. This fast regime is followed by a slower exponential decorrelation of the cluster sizes, with a characteristic time of about $4\, t_D$. The long time regime reflects in-coming contributions from distant particles approaching the cluster by diffusion and also escape events of more "stable" cluster particles attached by several bonds. Concerning the rate of in-coming particles by diffusion, for a volume fraction $\phi = 0.025$ and taking as reference a

[1]The Kramer escape time is $\tau_E = (1/D)[\int_{x_1}^{x_2} \exp(-\beta U) dx][\int_{x_{\min}}^{x_2} \exp(\beta U) dx]$ where $x_1 < x_{\min} < x_2$ and $U(x_1) = 0$, $dU(x_{\min})/dx = 0$ and $U(x_2) = 0$

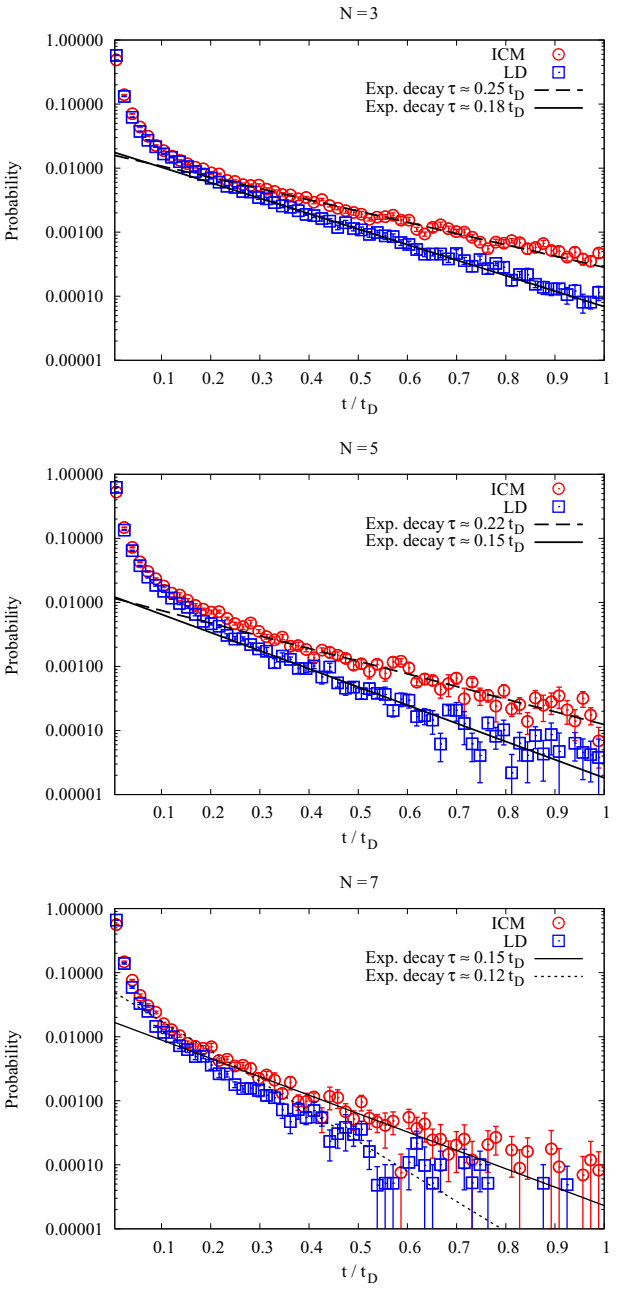

FIG. 9. Probability of survival times for three different sizes of clusters. Results are presented for ICM (red) and LD (blue). The error bars represent the standard error. Results obtained for potential 1.

colloidal radius of $R = 1.82$, the typical free path is about half $R\,[(4\pi/3)/\phi]^{1/3}$ (i.e., about 5 length units), while a relaxation time of about $5\,t_D$ corresponds to a diffusive excursion of a single colloid over 4 length units. However, the Kramer escape time for a particle attached with two bonds is about $\tau_E \approx 3.2\,t_D$ (estimated by using $2\,U(x)$ in the Kramer's expression for the potential 1). Thus, we conclude that the long-time decorrelation of the cluster sizes observed in these systems (having

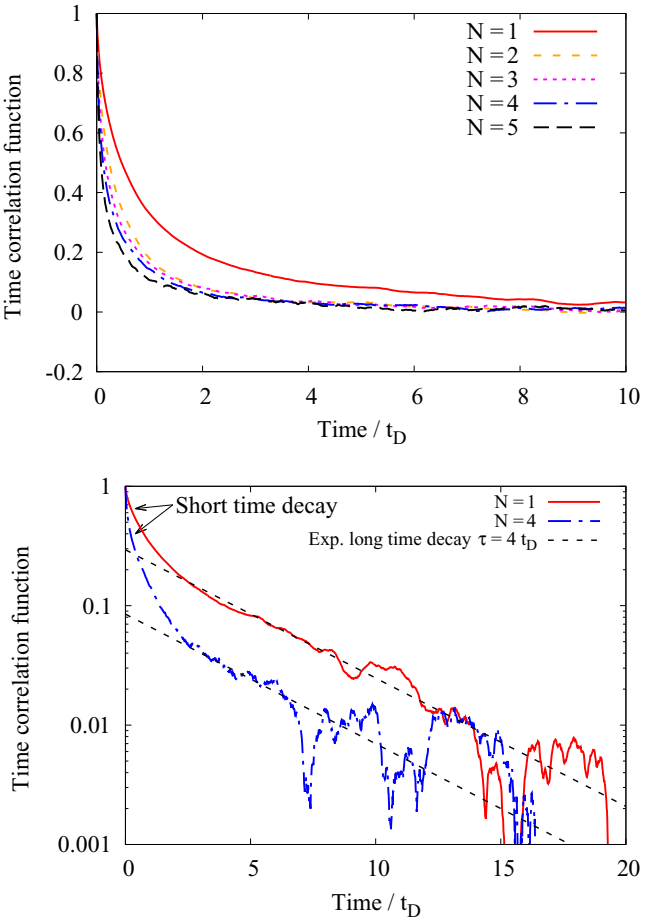

FIG. 10. Results from ICM simulations. Top: time correlation function of the number of clusters of sizes 1,2,3,4, and 5. Bottom: the same function has been drawn with the axis y in logarithmic scale. For clarity, just two different size of clusters have been depicted. Results obtained for potential 1.

a reduced number of particles) correspond to in-coming and out-going events of mainly individual colloids, which take place at similar rates (as it should in chemical equilibrium).

Similar relaxation rates are observed in the time correlation of the total mass of clusters having $N > N_{\text{ref}}$ (large clusters) or $N \leqslant N_{\text{ref}}$ (small clusters), where N_{ref} is some arbitrary reference number (we studied $N_{\text{ref}} = 5, 10$). Results for $N_{\text{ref}} = 5$ are plotted in Fig. 11 showing a long time relaxation rate of $5.7\,t_D$. Results for $N_{\text{ref}} = 10$ show a similar decay.

As Fig. 12 illustrates, a clear effect of hydrodynamics is to slow down the aggregation dynamics in this "long time" regime: while we find $\tau \approx 5.5\,t_D$ in simulations with hydrodynamics (ICM) the result of LD (no hydrodynamics) is $\tau \approx 3.5\,t_D$. Such slow down arises from the reduced mobility of the mutual mobility of close-by colloids. The mutual mobility of our hydrodynamic model is consistent with the Rotne-Prager-Yamakawa tensor, whose normal mobility at contact (distance $d = 2R$) is reduced by a factor somewhat larger than 2 with respect to the Stokes bulk value [22]. The reduction in mutual mobility becomes rather small for $d > 3R$, so this effect is mainly local and it probably does not significantly alter the rate of incoming particles. However, it certainly increases the average escape time, which is *inversely* proportional to the local mobility.

We have also analyzed the time-correlation function of the asphericity parameter, shown in Fig. 13 for cluster of size $N = 3$ and $N = 5$. Fast reorganizations or fluctuations of the cluster

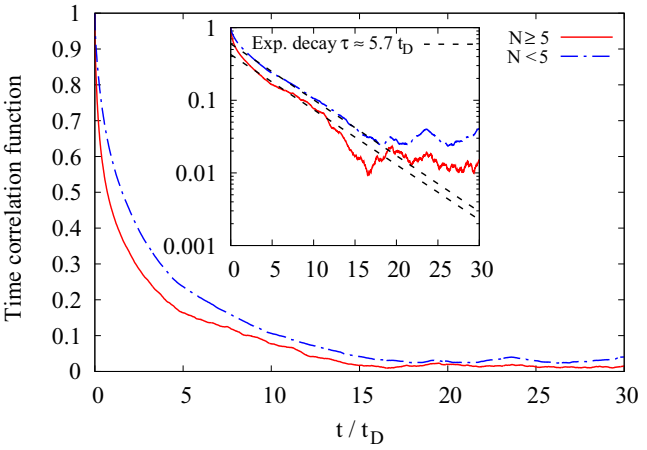

FIG. 11. Results from ICM simulations: time correlation function of the number of big ($N \geqslant 5$) and small ($N < 5$) clusters. In the inset, the same graph have been drawn with the y axis in logarithmic scale. In the latter case, for clarity, just two of the curves have been depicted. Results obtained for potential 1.

shape take place at times ($\approx 0.9 t_D$) in the same range of the short-time dynamics in cluster size. At longer times we could not extract statistics, simply because the short survival times of individual clusters. Interestingly, hydrodynamics also affects the rate of local reorganization of the cluster shape, although it does not alter the average asphericity.

V. CONCLUSION

We have analyzed a small system of colloidal particles ($N_T = 20, 40$) under short-ranged depletion interaction which reproduces the system considered by Whitmer and Luijten [9]. By contrast, we do not find any significant effect of hydrodynamics in the cluster size distribution or shape. The depletion potentials considered are mild, corresponding to fully reversible aggregation and formation of small clusters. In this scenario, the cluster size distribution and shape should

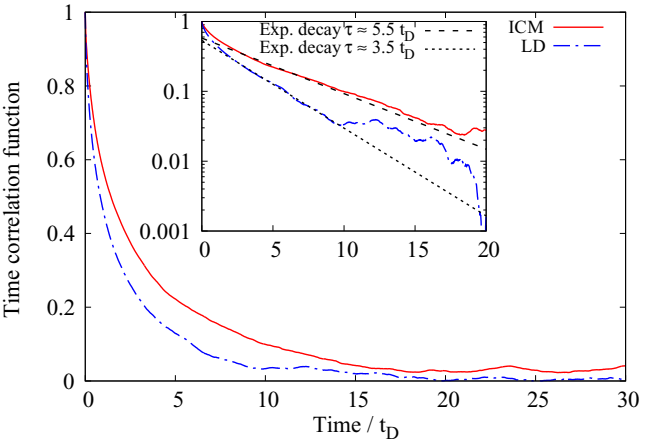

FIG. 12. Time correlation function of the total number of clusters of size N. The case $N = 1$ indicates detachment/attachment events of single particles. Results with ICM and LD simulations are shown. In the inset, the same graph with the y axis in logarithmic scale. Results obtained for potential 1.

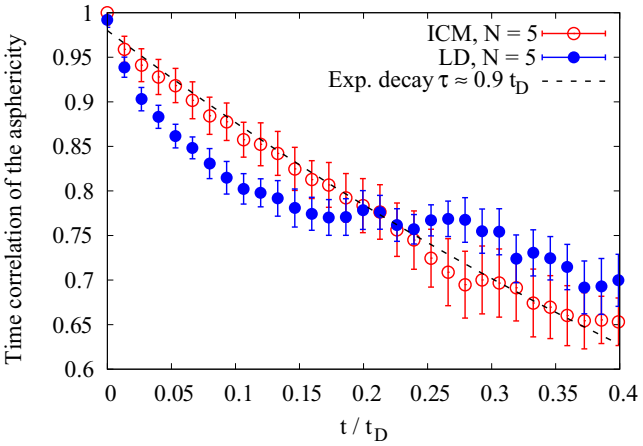

FIG. 13. Results from ICM simulations. Time correlation function of the asphericity for clusters of size $N = 3, 5$. Results obtained for potential 1. The error bars represent the standard error.

be determined by the chemical equilibrium or, equivalently, by the Gibbs-Boltzmann distribution associated to the colloidal free energy. The well-known Einstein relation between thermal energy, friction and diffusion $D = k_B T/\xi$, proves that changes in mobility (or friction) will not modify the *equilibrium* distribution. In this respect, our results are consistent. A possible way to create a deviation from equilibrium sustained over long times is a severe reduction of mobility. The mutual mobility (between pair of colloids) introduced by our hydrodynamic model [23] is similar to the Rotne-Prager approximation [22]. Thus, we do not resolve the lubrication regime (large increase in friction when particles are very close). Our results including lubrication interactions [24] indicate an increase in the Kramer escape time in some factor (about two) with respect to the present model. In any case, such times are still almost two orders of magnitude smaller than the sampling time we used here ($100\,t_D$) and cannot explain large differences between equilibrium and "hydrodynamically frustrated" structures. We thus conclude that in the system considered by Whitmer and Luijten, hydrodynamics cannot alter cluster size and shape over long times. We hypothesize that hydrodynamic effects could be sustained over longer times (frustration) in irreversible aggregation, but this issue is still under debate. A second conclusion of this work is the need to establish comparisons between hydrodynamic models and to further investigate their inherent limitations. A good example of such work can be found in Ref. [25]. In this respect, at short distances between particles, MPC brings out several artifacts such as a low Schmidt number [25] and also spurious depletion forces induced by the hydrodynamic solvent [26]. To precisely follow the parameters used in Ref. [9], in this work we have used $\mathrm{Sc} = 50$, which is not the Stokes limit regime $\mathrm{Sc} \to \infty$ of colloidal dynamics, but it is still large enough to expect small variations from the Einstein-Stokes diffusion, as shown in Ref. [27]. However, it is now known that the discrete nature of the MPC solvent introduces artificial depletion between colloidal particles [25]. A recent work by Wagner and Ripoll [26] studies these spurious depletion forces in MPC and propose ways to correct this artifact. Notably, this issue might explain putative spurious hydrodynamic effects in the work by Whitmer and Luijten [9]. It is relevant to say that many other works on colloidal aggregation (Refs. [9,11,12,14] is just a subset) have been performed using versions of the MPC or SRD-MD methods, which are similar and share this spurious drift induced by the discrete nature of the solvent. An indication of this possibility is the work by Tomilov et al. [11], which compares the diffusion coefficient of clusters of size N using BDHI (based on Rotne-Prager-Yamakawa mobility), BD (no-hydrodynamics), and MPC. They find $D_N \sim 1/N$ for BD, and $D_N \sim N^{-0.37}$ for BDHI, while $D_N \sim N^{-0.59}$ for SRD-MD. The globular shape of these clusters (note that $R(N) \sim N^{1/3}$ for a perfect globule) should lead to a Zimm (hydrodynamic) diffusion proportional

to the cluster radius (consistent with the BDHI result $D_N \propto 1/R(N) \sim N^{-0.37}$). By contrast MPC creates more open structures $D_N \sim N^{-0.59}$, which qualitatively agree with the "elongated structures" found by Whitmer and Luijten. It could well be that both arise from the spurious lubrication of uncorrected versions of the MPC method (see Ref. [26] for technical discussion and strategies to avoid MPC-induced depletion). A second important issue, which is often overlooked in the literature of aggregation simulation, is the need for large enough sampling times, both to gather statistics and also to reach the stationary regime (if it exists), where transient hydrodynamic effects are finally forgotten. In summary, more studies are still needed to unveil the hydrodynamic effects on colloidal aggregation, and these should probably include a refined model for lubrication. Beyond hydrodynamics, depletion and DLVO forces are usually modeled using pair-wise potentials, which completely neglect the many-body nature of such effective interactions. Many-body effects might well be relevant within large or moderately large clusters.

ACKNOWLEDGMENTS

The authors acknowledge the financial support from MINECO (Spain) under Grant No. FIS2017-86007-C3-1-P and from the American Chemical Society Petroleum Research Funding, under Grant No. 54312-ND9.

[1] M. T. A. Bos and J. H. J. van Opheusden, Brownian dynamics simulation of gelation and aging in interacting colloidal systems, Phys. Rev. E **53**, 5044 (1996).
[2] M. Mellema, J. H. J. Van Opheusden, and T. Van Vliet, Relating colloidal particle interactions to gel structure using Brownian dynamics simulations and the Fuchs stability ratio, J. Chem. Phys. **111**, 6129 (1999).
[3] M. Whittle and E. Dickinson, Brownian dynamics simulation of gelation in soft sphere systems with irreversible bond formation, Mol. Phys. **90**, 739 (1997).
[4] E. Dickinson, Structure and rheology of simulated gels formed from aggregated colloidal particles, J. Colloid Interface Sci. **225**, 2 (2000).
[5] J. F. M. Lodge and D. M. Heyes, Rheology of transient colloidal gels by Brownian dynamics computer simulation, J. Rheol. **43**, 219 (1999).
[6] R. Yamamoto, K. Kim, Y. Nakayama, K. Miyazaki, and D. R. Reichman, On the role of hydrodynamic interactions in colloidal gelation, J. Phys. Soc. Jpn. **77**, 084804 (2008).
[7] Y. Nakayama and R. Yamamoto, Simulation method to resolve hydrodynamic interactions in colloidal dispersions, Phys. Rev. E **71**, 036707 (2005).
[8] A. Furukawa and H. Tanaka, Key Role of Hydrodynamic Interactions in Colloidal Gelation, Phys. Rev. Lett. **104**, 245702 (2010).
[9] J. K. Whitmer and E. Luijten, Influence of hydrodynamics on cluster formation in colloid-polymer mixtures, J. Phys. Chem. B **115**, 7294 (2011).
[10] P. J. Lu, E. Zaccarelli, F. Ciulla, A. B. Schofield, F. Sciortino, and D. A. Weitz, Gelation of particles with short-range attraction, Nature **453**, 499 (2008).
[11] A. Tomilov, A. Videcoq, M. Cerbelaud, M. A. Piechowiak, T. Chartier, T. Ala-Nissila, D. Bochicchio, and R. Ferrando, Aggregation in colloidal suspensions: Evaluation of the role of hydrodynamic interactions by means of numerical simulations, J. Phys. Chem. B **117**, 14509 (2013).
[12] A. M. Laganapan, M. Mouas, A. Videcoq, M. Cerbelaud, M. Bienia, P. Bowen, and R. Ferrando, How colloid-colloid interactions and hydrodynamic effects influence the percolation threshold: A simulation study in alumina suspensions, J. Colloid Interface Sci. **458**, 241 (2015).
[13] C. P. Royall, J. Eggers, A. Furukawa, and H. Tanaka, Probing Colloidal Gels at Multiple Length Scales: The Role of Hydrodynamics, Phys. Rev. Lett. **114**, 258302 (2015).
[14] X. J. Cao, H. Z. Cummins, and J. F. Morris, Hydrodynamic and interparticle potential effects on aggregation of colloidal particles, J. Colloid Interface Sci. **368**, 86 (2012).

[15] Z. Varga, G. Wang, and J. Swan, The hydrodynamics of colloidal gelation, Soft Matter **11**, 9009 (2015).
[16] Z. Varga and J. Swan, Hydrodynamic interactions enhance gelation in dispersions of colloids with short-ranged attraction and long-ranged repulsion, Soft Matter **12**, 7670 (2016).
[17] F. B. Usabiaga, R. Delgado-Buscalioni, B. E. Griffith, and A. Donev, Inertial coupling method for particles in an incompressible fluctuating fluid, Comput. Methods Appl. Mech. Eng. **269**, 139 (2014).
[18] S. Asakura and F. Oosawa, On interaction between two bodies immersed in a solution of macromolecules, J. Chem. Phys. **22**, 1255 (1954).
[19] M. P. Allen and D. J. Tildesley, *Computer Simulation of Liquids* (Oxford University Press, Oxford, 1989).
[20] C. S. Peskin, The immersed boundary method, Acta Numerica **11**, 479 (2002).
[21] H. Risken, *Fokker-Planck Equation* (Springer, Berlin, 1996), p. 63.
[22] A. Vázquez-Quesada, F. B. Usabiaga, and R. Delgado-Buscalioni, A multiblob approach to colloidal hydrodynamics with inherent lubrication, J. Chem. Phys. **141**, 204102 (2014).
[23] F. Balboa Usabiaga, Fluam, https://github.com/fbusabiaga/fluam.
[24] Yu Mingzhou and R. Delgado-Buscalioni, The effect of hydrodynamic interactions on the dynamics and equilibrium configuration of colloidal aggregates in a quiescent flow regime (unpublished).
[25] D. S. Bolintineanu, G. S. Grest, J. B. Lechman, F. Pierce, S. J. Plimpton, and P. R. Schunk, Particle dynamics modeling methods for colloid suspensions, Comp. Part. Mech. **1**, 321 (2014).
[26] M. Wagner and M. Ripoll, Solvent-induced depletion interactions in multiparticle collision dynamic simulations, Int. J. Mod. Phys. C **30** 1941008 (2019).
[27] F. Balboa Usabiaga, X. Xie, R. Delgado-Buscalioni, and A. Donev, The Stokes-Einstein relation at moderate schmidt number, J. Chem. Phys. **139**, 214113 (2013).